Article

Chiral Phase Transition in Two-Dimensional Supramolecular Assemblies of Prochiral Molecules

Franck Vidal, Erik Delvigne, Sebastian Stepanow, Nian Lin, Johannes V. Barth, and Klaus Kern

J. Am. Chem. Soc., **2005**, 127 (28), 10101-10106• DOI: 10.1021/ja0525049 • Publication Date (Web): 25 June 2005

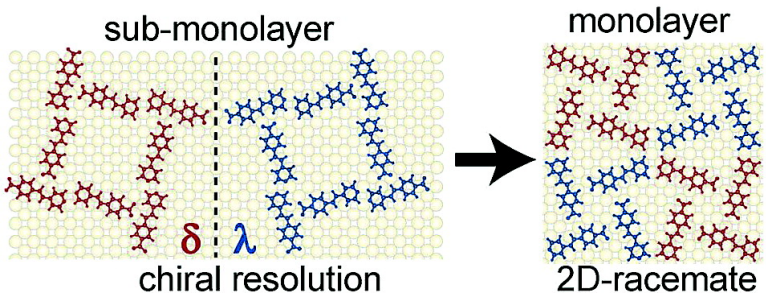

More About This Article

Additional resources and features associated with this article are available within the HTML version:

- Supporting Information
- Links to the 18 articles that cite this article, as of the time of this article download
- Access to high resolution figures
- Links to articles and content related to this article
- Copyright permission to reproduce figures and/or text from this article

View the Full Text HTML

J|A|C|S
ARTICLES
Published on Web 06/25/2005

Chiral Phase Transition in Two-Dimensional Supramolecular Assemblies of Prochiral Molecules

Franck Vidal,[†] Erik Delvigne,[‡] Sebastian Stepanow,[†] Nian Lin,*[,†] Johannes V. Barth,[‡,§] and Klaus Kern[†,‡]

Contribution from the Max-Planck-Institut für Festkörperforschung, Heisenbergstrasse 1, D-70569 Stuttgart, Germany, Institut de Physique des Nanostructures, Ecole Polytechnique Fédérale de Lausanne, CH-1015 Lausanne, Switzerland, and Departments of Chemistry and Physics & Astronomy, The University of British Columbia, Vancouver, BC V6T 1Z4, Canada

Received April 18, 2005; E-mail: n.lin@fkf.mpg.de

Abstract: The self-assembly of the rodlike two-dimensional chiral molecule 4-[*trans*-2-(pyrid-4-yl-vinyl)] benzoic acid on the Cu(100) surface has been investigated by scanning tunneling microscopy. Upon adsorption at $T \geq 300$ K, the molecules are deprotonated and assemble in parquet patterns when the coverage remains below a critical value. Corresponding high-resolution data reveal that the ordering implies mesoscopic chiral resolution as a result of chiroselective interactions (i.e., two domains comprise exclusively one enantiomer). When the critical coverage is exceeded, an abrupt transition to a single racemic phase is observed with a different lateral molecular coupling scheme. The shifting of the subtle balance between the weak lateral coupling, substrate bonding, and the packing requirements encountered with the increased molecular coverage is suggested to be the driving force for this homochiral-to-heterochiral phase transition.

1. Introduction

2D chiral systems consisting of chiral or prochiral molecular building blocks adsorbed at surfaces have been studied intensively over the past few years in view of their unique properties and technical relevance (e.g., in enantioselective heterogeneous catalysis[1,2] or nonlinear optics).[3] Recent studies conducted under ultrahigh vacuum conditions using scanning tunneling microscopy (STM) revealed in exquisite detail that complex organic molecules frequently organize in a wide variety of chiral phases upon adsorption on metal surfaces.[4,5] In particular, chiral recognition and resolution can occur in the self-assembly of racemic mixtures of both chiral molecules and prochiral species whose chirality is induced by the 2D confinement at a surface. As a result, distinct homochiral arrangements evolve, such as clusters,[6−11] 1D arrangements,[12−18] and 2D extended domains.[2,19−22] Chiral resolution reflects chiroselective interaction mediated by noncovalent interactions such as hydrogen bonds, electrostatic forces, van der Waals interactions, and metal−ligand interactions. Furthermore, the atomic structure of the substrates influences the ordering since the adsorbed molecules usually prefer specific adsorption sites and orientations. Because the balance of all these effects determines the final situation, a subtle change in one of them is able to shift the potential landscape and lead to different thermal equilibrium configurations.

In this article, we present a scanning tunneling microscopy (STM) study of a system where mesoscopic chiral resolution in assembly of 2D chiral rodlike molecules is effective only under the condition that the molecular coverage remains below a critical value. For higher coverages, the molecules form a

[†] Max-Planck-Institut für Festkörperforschung.
[‡] Ecole Polytechnique Fédérale de Lausanne.
[§] The University of British Columbia.

(1) Baiker, A.; Blaser, H. U. In *Handbook of Heterogeneous Catalysis*; Ertl, G., Knözinger, H., Weitkamp, J., Eds.; VCH: Weinheim, Germany, 1997; Vol. 5, pp 2422−2430.
(2) Lorenzo, M. O.; Baddeley, C. J.; Muryn, C.; Raval, R. *Nature* **2000**, *404*, 376.
(3) Verbiest, T.; Elshocht, S. V.; Kauranen, M.; Hellemans, L.; Snauwaert, J.; Nuckolls, C.; Katz, T. J.; Persoons, A. *Science* **1998**, *282*, 913.
(4) Barlow, S. M.; Raval R. *Surf. Sci. Rep.* **2003**, *50*, 201−341 and references therein.
(5) Humblot, V.; Barlow, S. M.; Raval R. *Prog. Surf. Sci.* **2004**, *76*, 1 and references therein.
(6) Böhringer, M.; Morgenstern, K.; Schneider, W.-D.; Berndt, R. *Angew. Chem., Int. Ed.* **1999**, *38*, 821.
(7) Böhringer, M.; Morgenstern, K.; Schneider, W.-D.; Berndt, R.; Mauri, F.; Vita, A. D.; Car, R. *Phys. Rev. Lett.* **1999**, *83*, 324.
(8) Messina, P.; Dmitriev, A.; Lin, N.; Spillmann, H.; Abel, M.; Barth, J. V.; Kern K. *J. Am. Chem. Soc.* **2002**, *124*, 14000.
(9) Kühnle, A.; Linderoth, T. R.; Hammer, B.; Besenbacher, F. *Nature* **2002**, *415*, 891.
(10) Jonkheijm, P.; Miura, A.; Zdanowska, M.; Hoeben, F. J. M.; De Feyter, S.; Schenning, A. P. H. J.; De Schryver, F. C.; Meijer, E. W. *Angew. Chem., Int. Ed.* **2004**, *43*, 74.
(11) Kühnle, A.; Linderoth, T. R.; Besenbacher, F. *J. Am. Chem. Soc.* **2003**, *125*, 14680.
(12) Barth, J. V.; Weckesser, J.; Cai, C.; Günter, P.; Bürgi, L.; Jeandupeux, O.; Kern, K. *Angew. Chem.* **2000**, *112*, 1285 (*Int. Ed.* **2000**, *39*, 1230).
(13) Weckesser, J.; De Vita, A.; Barth, J. V.; Cai, C.; Kern, K. *Phys. Rev. Lett.* **2001**, *87*, 096101.
(14) Barth, J. V.; Weckesser, J.; Trimarchi, G.; Vladimirova, M.; De Vita, A.; Cai, C.; Brune, H.; Günter, P.; Kern, K. *J. Am. Chem. Soc.* **2002**, *124*, 7991.
(15) Humblot, V.; Haq, S.; Muryn, C.; Hofer, W. A.; Raval, R. *J. Am. Chem. Soc.* **2002**, *124*, 503.
(16) Chen, Q.; Frankel, D. J.; Richardson, N. V. *Langmuir* **2002**, *18*, 3219.
(17) Chen, Q.; Richardson, N. V. *Nat. Mater.* **2003**, *2*, 324.
(18) Böhringer, M.; Schneider, W.-D.; Berndt, R. *Angew. Chem., Int. Ed.* **2000**, *39*, 792.
(19) Spillmann, H.; Dmitriev, A.; Lin, N.; Messina, P.; Barth, J. V.; Kern, K. *J. Am. Chem. Soc.* **2003**, *125*, 10725.
(20) Dmitriev, A.; Spillmann, H.; Lingenfelder, M.; Lin, N.; Barth, J. V.; Kern, K. *Langmuir* **2004**, *20*, 4799.
(21) Fasel, R.; Parschau, M.; Ernst, K.-H. *Angew. Chem., Int. Ed.* **2003**, *42*, 5178.
(22) France, C. B.; Parkinson, B. A. *J. Am. Chem. Soc.* **2003**, *125*, 12712.

10.1021/ja0525049 CCC: $30.25

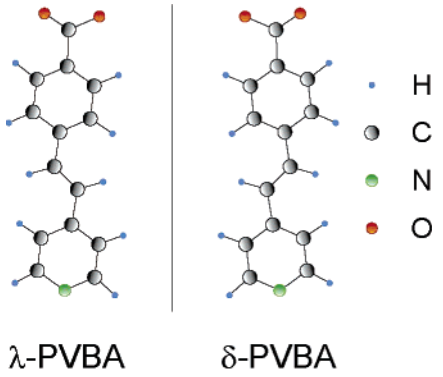

Figure 1. Chemical structure of PVBA. The 2D chiral species encountered upon adsorption are labeled λ and δ.

racemic layer. These findings are related to earlier low-temperature STM observations from Böhringer et al., who reported a chiral phase transition dependent on molecular coverage for the case of nitronaphthalene molecules on Au(111).[18] At low coverage, nitronaphthalene forms 1D homochiral double chains. With increasing coverage, a racemate structure gradually developed where the homochiral phase and the heterochiral phase coexist. The driving forces were associated with the preferred molecular adsorption at different sites of the inhomogeneous substrate and intricate intermolecular electrostatic interactions. However, with the present system we find a rather sharp phase transition on a homogeneous square substrate, where homochiral phases are present exclusively until a critical coverage and the transition to the new heterochiral phase is completed within a very narrow coverage range. The driving force governing the transition is ascribed to the packing constraints at the high molecular coverage overriding repulsive intermolecular interactions.

We employed the molecule 4-[*trans*-2-(pyrid-4-yl-vinyl)] benzoic acid (PVBA), which has been designed for nonlinear optics applications.[23,24] PVBA is a rigid and planar species comprising a pyridyl moiety (which will be referred to as "head" in the following) and a carboxylic acid moiety ("tail") linked together by an ethenylene bridge. The free molecule has a length of 12.5 Å and is prochiral in the gas phase. Upon adsorption at a metal surface, the angled structure related to the ethenylene C−C bond imposes 2D chirality[12−14] (see Figure 1; this is a pure consequence of 2D confinement). The adsorption and supramolecular self-assembly of PVBA at different metallic substrates have been studied previously. On Pd(110), the molecule−substrate interactions dominate and no chiral ordering phenomena were observed.[25,26] On Ag(110), PVBA induces a mesoscopic arrangement of regular chiral steps.[27] On Ag(111), it was found that PVBA self-assembles into homochiral twin chains running along high-symmetry directions of the substrate lattice.[12−14] These chains are composed of PVBA enantiomers whose coupling is mediated by sequential head-to-tail hydrogen-bonding between carboxylic acid and pyridyl moieties and weak chiroselective lateral interactions. The binding energy of the dominating O−H···N bonds was estimated to ∼9.2 kcal/mol (0.4 eV) per molecule.[14] With the self-assembly of PVBA on Cu(100), the chemical reactivity of the substrate plays an important role. It has been shown that deprotonation of carboxylic acids typically occurs on copper surface at intermediate temperatures.[28−30] In the present case, X-ray photoemission spectroscopy data indicate that PVBA's carboxylic group readily undergoes deprotonation upon deposition on Cu(100) which is at room temperature,[31] that is, the benzoate species is formed, to which PVBA refers in the following. An important consequence of the deprotonation is that it prevents head-to-tail hydrogen bonding. However, the benzoate and the pyridyl moiety can be engaged in intermolecular coupling schemes through weak hydrogen bonding to adjacent molecules' aromatic rings.[30]

2. Experimental Section

Sample preparation and characterization have been conducted in a home-built ultrahigh vacuum (UHV) STM system (base pressure ∼3 × 10^{-10} mbar).[32] The Cu(100) surface was cleaned by repeated cycles of Ar^+ sputtering and subsequent annealing at 800 K. This procedure led to the formation of atomically flat terraces of up to 200-nm width. The synthesis of the PVBA molecules is described in refs 23 and 24. The PVBA sample in powder form was deposited by organic molecular beam epitaxy (OMBE) from a Knudsen-cell type evaporator. The temperature of the cell was held at (445.0 ± 0.2) K, and the Cu(100) surface was at 300 K during deposition. Upon annealing the samples for a few minutes at temperatures between 400 and 450 K and subsequent cooling to 300 K, we performed *in situ* STM measurements at 300 K in the constant current mode with a typical tunneling current of 1 nA and bias voltage of 0.5 V. The observed STM topography remained unaffected by the STM measurement after several consecutive scans of the same area. The deposition rate was calibrated from the molecular coverage in 200 × 200 nm^2 STM images taken at different spots of the sample and is ∼0.0036 PVBA × Cu $atom^{-1}$ × min^{-1}. We define a coverage of 0.05 PVBA × Cu $atom^{-1}$ as the critical coverage (α_C).

3. Results and Discussion

3.1. Chiral Resolution in Parquet Patterns below the Critical Coverage. In Figure 2a, a typical STM topograph showing the ordering of PVBA below the critical coverage (0.36 α_C) is depicted. Two domains displaying different orientations can be distinguished in the upper and lower parts of Figure 2a, where the molecular axis is rotated by ∼11° or −11° away from the [001] substrate direction, respectively. The parquet domains comprise areas with "square voids" (region A in Figure 2a, for example) and "rectangular close-packed" arrangements (region B in Figure 2a) where the molecular density is apparently higher. These substructures are designated as types A and B, respectively. More insight into the PVBA packing in the domains can be gained from the high-resolution data in Figure 2b,c, where submolecular features of individual species are clearly resolved.

(23) Cai, C.; Bösch, M.; Müller, B.; Tao, Y.; Kündig, A.; Bosshard, C.; Gan, Z.; Biaggio, I.; Liakatas, I.; Jäger, M.; Schwer, H.; Günter, P. *Adv. Mater.* **1999**, *11*, 745.
(24) Cai, C.; Müller, B.; Weckesser, J.; Barth, J. V.; Tao, Y.; Bösch, M. M.; Kündig, A.; Bosshard, C.; Biaggio, I.; Günter, P. *Adv. Mater.* **1999**, *11*, 750.
(25) Weckesser, J.; Barth, J. V.; Kern, K. *J. Chem. Phys.* **1999**, *110*, 5351.
(26) Weckesser, J.; Barth, J. V.; Cai, C.; Müller, B.; Kern, K. *Surf. Sci.* **1999**, *431*, 168.
(27) Pascual, J. I.; Barth, J. V.; Ceballos, G.; Trimarchi, G.; De Vita, A.; Kern, K.; Rust, H.-P. *J. Chem. Phys.* **2004**, *120*, 11367.
(28) Perry, C. C.; Haq, S.; Frederick, B. G.; Richardson, N. V. *Surf. Sci.* **1998**, *409*, 512.
(29) (a) Lin, N.; Dmitriev, A.; Weckesser, J.; Barth, J. V.; Kern, K. *Angew. Chem., Int. Ed.* **2002**, 41, 4779. (b) Barth, J. V.; Weckesser, J.; Lin, N.; Dmitriev, A.; Kern, K. *Appl. Phys. A* **2003**, *76*, 645.
(30) Stepanow, S.; Strunskus, T.; Lingenfelder, M.; Dmitriev, A.; Spillmann, H.; Lin, N.; Barth, J. V.; Wöll, Ch.; Kern, K. *J. Phys. Chem. B* **2004**, *108*, 19392.
(31) Strunskus, T.; Wöll, Ch. University of Bochum, 2004; Private communication.
(32) Brune, H.; Röder, H.; Bromann, K.; Kern, K. *Thin Solid Films* **1995**, *264*, 230.

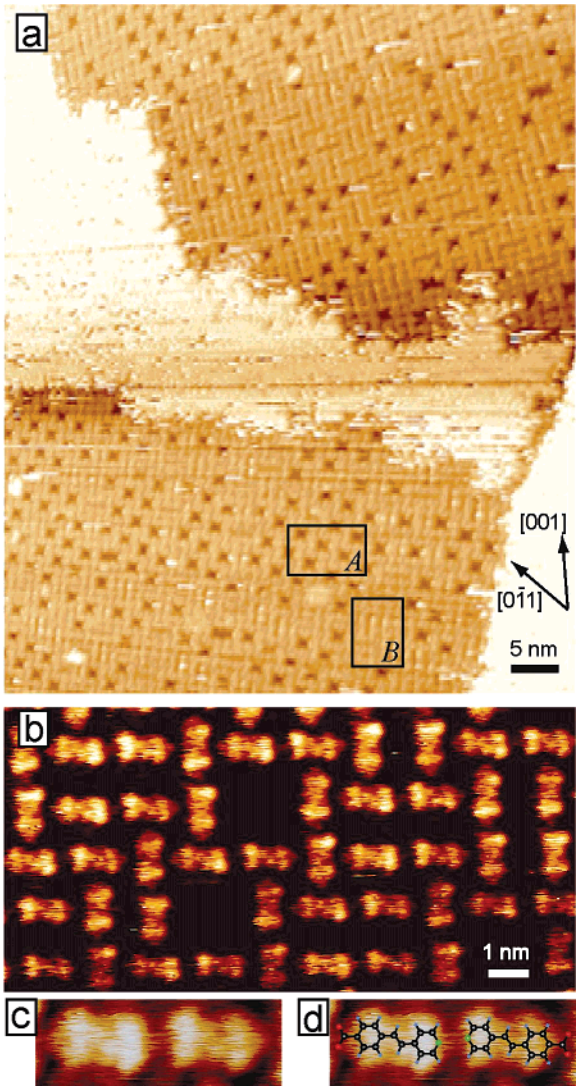

Figure 2. (a) STM topograph of a PVBA parquet pattern assembled on Cu(100) for a coverage of 0.36 α_C. Regions A and B indicate areas where different local substructures are distinguished. (b,c) High-resolution images of a chiral domain built from δ-PVBA. (d) Structural model of PVBA superimposed on the high-resolution data revealing the chiral resolution.

The molecules are imaged as 1.5-Å-high dog-bone protrusions with a length of ~12 Å. The apparent height is a typical value for planar aromatic molecules with a π-electrons system oriented parallel to the surface.[25,33−35] The shape and extension of the imaged molecules agree with that of an isolated PVBA molecule, whose length is 12.3 Å in the unrelaxed configuration. This clearly suggests that PVBA is adsorbed in a flat-lying geometry, with the aromatic rings parallel to the surface.

Within the domains dimeric PVBA units prevail (cf. Figure 2b), that is, the two molecules form pairs with the long molecular axis aligning parallel in a row. This holds for both "horizontal" and "vertical" dimers which are identical and just 90° rotated, reflecting the fourfold symmetry of the Cu(100) surface. High-resolution data allow us to distinguish substructures within single molecules, as shown in Figure 2c. The side consisting of two main lobes and a nearly "evanescent" one is ascribed to the carboxylate moiety and the more flat side is ascribed to the pyridyl moiety, based on a careful comparison with high-resolution images of an Fe−PVBA metal−organic coordination network on the same surface.[36] Therefore, unambiguous correlation of the imaged inner structure with the molecular geometry could be achieved, allowing us to conclude that in a dimer two PVBA units are facing each other with their pyridyl moieties (i.e., in a head-to-head configuration), as shown by the model shown in Figure 2d. Note that the bonding length and observed orientation exclude a Cu-adatom mediated coupling of the dimers, which was encountered with related systems.[29] By contrast, this arrangement is similar to the one adopted for pyridine dimers as reported in the literature.[37] Moreover, the high-resolution images allow for the determination of the chirality of individual molecules (cf. Figure 2b,c), and a systematic scrutiny of submolecular-resolution STM data clearly reveals that the two PVBA units in a dimer always display the same handedness.

As shown in Figure 2a, the dimers are organized in domains covering entire terraces as large as 100 nm. In the corresponding parquet pattern no distinct unit cell can be defined, and there is similarly no regular long-range ordering. Nevertheless, some key features are universally encountered. First, the linear molecular packing is restricted to the dimers, that is, there are no longer segments or continuous chains, rather the endgroups of the dimer molecules always point to centers of adjacent PVBA. This is in agreement with the expected repulsion between the negative carboxylate groups terminating both ends of the dimers and the endgroups of neighboring molecules. Second, the domains are exclusively built out of dimers from one PVBA enantiomer, as exemplified in Figure 2b, where a δ-PVBA domain is depicted. This similarly holds for λ-PVBA domains. Consequently, the domains are enantiomerically pure homochiral phases.

Models for the packing of the δ-PVBA and λ-PVBA domains based on high-resolution STM images are depicted in Figure 3. We assumed an unrelaxed configuration of the PVBA carboxylate and the absence of adsorption-induced reconstruction of the copper substrate. Following results from DFT calculations indicating that benzene adsorbs at hollow sites on Cu(100),[38] the aromatic rings bearing the carboxylate moieties were assumed to be located at 4-fold hollow sites of the Cu(100) substrate. The N atom of the pyridyl moiety is then located in near-bridge site. The homochiral models fit properly with the STM data when superimposed on the latter, as shown in Figure 3a,b, validating our assumption of chiral resolution in domain formation. Moreover, it can be seen from the propeller-shaped features in Figure 3a,b that the two domains comprise mirror-symmetric motifs. These motifs, which can be found at the junctions between squares, are always turning counterclockwise in the δ-PVBA domain (Figure 3a) and clockwise in the λ-PVBA domain (Figure 3b). They are designated left-turning (L) and right-turning (R), respectively. The L motif is turned clockwise compared to the [001] direction, and the R motif is turned counterclockwise. The dimers' orientation is inferred from the model by defining it as the axis across the center of

(33) Sautet, P. *Chem. Rev.* **1997**, *97*, 1097.
(34) Dmitriev, A.; Lin, N.; Weckesser, J.; Barth, J. V.; Kern, K. *J. Phys. Chem. B* **2002**, *106*, 6907.
(35) Lippel, P. H.; Wilson, R. J.; Miller, M. D.; Woell, Ch.; Chiang, S. *Phys. Rev. Lett.* **1989**, *62*, 171.
(36) Lin, N.; Stepanow, S.; Vidal, F.; Barth, J. V.; Kern, K. *Chem. Commun.* **2005**, 1681.
(37) Coussan, S.; Brenner, V.; Perchard, J. P.; Zheng, W. Q. *J. Chem. Phys.* **2000**, *113*, 8059.
(38) Lorente, N.; Hedouin, M. F. G.; Palmer, R. E.; Persson, M. *Phys. Rev. B* **2003**, *68*, 155401.

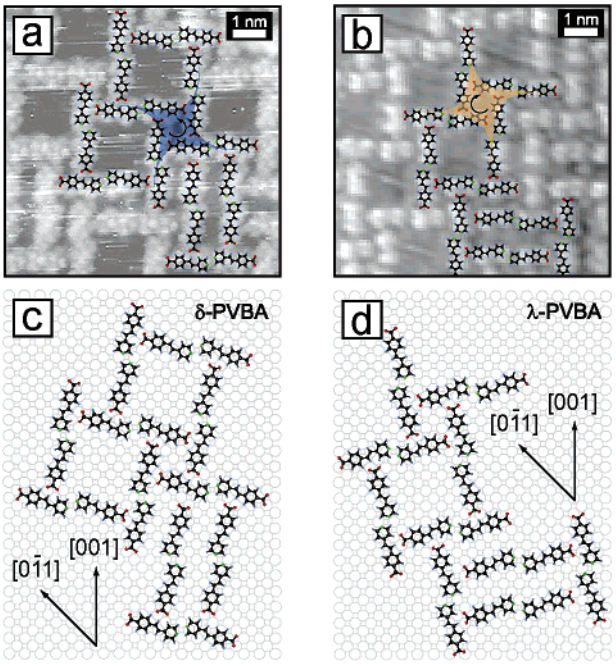

Figure 3. (a,b) STM topographs of the two homochiral arrangements in enantiopure parquet pattern domains. The junctions between squares are always turning counterclockwise in the δ-PVBA domain (in blue) and clockwise in the λ-PVBA domain (in yellow). (c,d) Corresponding models with δ-PVBA and λ-PVBA.

the molecules' phenyl rings. As a result, we find that the dimers are oriented in the [015] and [0$\bar{5}$1] directions for the L domains and in the [051] and [0$\bar{1}$5] directions for the R domains. This corresponds to rotations of the dimers by 11.3° and −11.3° with respect to the [001] direction, in good agreement with the STM observations. Thus, the chiral motifs of L and R domains are built by δ-PVBA and λ-PVBA, respectively. The Cu(100) substrate has a fourfold symmetry, allowing in principle for a total of eight different arrangements: two chiral arrangements, both of which can have four different rotated representations. However, since the parquet domains are built from perpendicular dimers, 90° or 180° rotations are redundant and we can only distinguish the sketched L and R domains. Thus, two levels of chirality are encountered: molecular point chirality (i.e., adsorption-induced symmetry breaking) and mesoscopic organizational chirality (homochiral dimers and homochiral domains). On the macroscopic scale, the surface, being covered by a mixture of homochiral domains, remains racemic.

We now focus on the intermolecular coupling of the PVBA units. Potential hydrogen bonds are depicted in Figure 4a. Estimated distances and angles between the atoms, as determined from this model using unrelaxed configurations, are displayed in Table 1. These values are comparable with those found in other systems where weak hydrogen bonding interactions are responsible for structural arrangements. Although C−H···O bonds are considerably weaker than O−H···O or O−H···N hydrogen bonds, they are ubiquitous in macromolecular systems and have an important impact on the packing of many organic crystals.[39,40] Ab initio calculations indicate that C−H···O interactions between CH_4 and oxygen in water molecules have a binding energy of a 0.3 kcal/mol.[41] Experimental data supported by ab initio calculations show that the binding energy can reach ∼1.72 kcal/mol for the case of 4-methoxybenzaldehyde dimers in the liquid phase with O−H distances of 2.46 and 3.16 Å.[42] In addition, the C−H···O bonds are less directional than O−H···O bonds.[41] These features signal that C−H···O bonding can be invoked to explain the ordering of the PVBA molecules with the present system. In the case of PVBA molecules self-assembled in twin chains at the Ag(111) surface, a lateral cohesive energy of 2.1 kcal/mol (90 meV) per molecule was estimated, where the O···H distance in the potential lateral C−H···O hydrogen bonds was ∼2.8 Å, comparable to some of the distances obtained from the modeling in the present case. Moreover, since carboxylate moieties exist in the present case we expect significantly increased binding energies as the charged oxygen atoms of the carboxylate moieties are stronger hydrogen bond acceptors (note that this effect might be partially leveraged by screening from the metal substrate). It is worthwhile to point out that the 90° lateral bonding is similar to those encountered in PTCDA and NTCDA systems assembled at various surfaces.[43] Concerning the pyridyl groups, the C−H···N binding energy can be of the same order of magnitude as that of C−H···O bonds with neutral oxygen.[44] Specifically, with pyridine dimers, DFT calculations indicate a H···N distance of 2.6 Å and a modest C−H···N binding energy of 1.32 kcal/mol.[37] Therefore, by comparing similar systems in 3D and 2D, the molecular arrangement observed here can be rationalized by weak C−H···O and possibly C−H···N coupling. Nevertheless, detailed calculations will be needed to clarify these points unambiguously.

The model in Figure 4a shows that the carboxylate groups of the horizontal PVBA can be engaged in bifurcated hydrogen bonds with a total of three hydrogen atoms of the vertical PVBA (one H atom of the pyridyl ring, one of the ethenylene backbone, and one of the phenylene ring).[45] On the left side, three of the four bond lengths (H···O distance) are around 2.0 Å (assuming an unrelaxed geometry), and the bond angles are close to 165°. On the right side, only one short bond length of ∼2.0 Å can be found, while the other three bond lengths are around 3.2 Å, implying that this configuration is less favorable. For three of the bonds on the right side the bond angles are ∼180°, which is favorable for the strength of the H-bonds. However, weak and moderate H-bonds only have weak directionality, meaning that the bond strength decreases only by a small amount when the bond angles deviate from 180°.[45] Therefore, bonding to the left side of molecules in an L domain is preferred. This argumentation is supported by a statistical analysis of STM data (based on 600 molecules), which indeed reveals that at 0.4 α_C approximately 76% of all carboxylate groups bond in the favorable configuration and only 24% in the less favorable one. If an ideal homochiral domain was built out of molecules that are bonding only to the favored side, the resulting structure would consist of connected propeller-shaped motifs leaving open squares between them (cf. Figure 3). This structure corresponds

(39) Desiraju, G. R.; Steiner, T. *The Weak Hydrogen Bond in Structural Chemistry and Biology*; Oxford University Press: Oxford, 1999.
(40) Desiraju, G. R. *Acc. Chem. Res.* **1996**, *29*, 441.
(41) Gu, Y.; Kar, T.; Scheiner, S. *J. Am. Chem. Soc.* **1999**, *121*, 9411.
(42) Ribeiro-Claro, P. J. A.; Batista De Carvalho, L. A. E.; Amado, A. M. *J. Raman Spectrosc.* **1997**, *28*, 867.
(43) Strohmaier, R.; Petersen, J.; Gompf, B.; Eisenmenger, W. *Surf. Sci.* **1998**, *418*, 91.
(44) Mazik, M.; Bläser, D.; Boese, R. *Tetrahedron* **2001**, *57*, 5791.
(45) Steiner, T. *Angew. Chem., Int. Ed.* **2002**, *41*, 48.

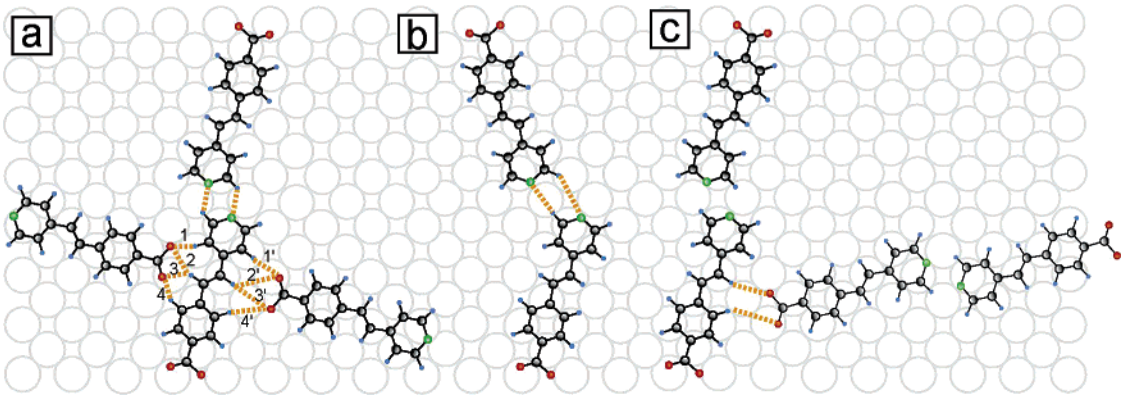

Figure 4. (a) Tentative model showing potential intermolecular hydrogen bonds for the preferred homochiral arrangement in the parquet pattern. (b,c) Models illustrating the poorer coupling encountered in hypothetical heterochiral configurations. In both cases significant larger distances of N···H and O···H are encountered.

Table 1. Values of the Distances and Angles between Atoms Involved in Potential Hydrogen Bonds Inside a Domain, Derived from the Model in Figure 4a Assuming an Unrelaxed Molecular Geometry[a]

C–H···Y	C–Y distance (Å)	H···Y distance (Å)	C–H···Y angle (deg)
C−H···N	2.95	2.2	127
C−H···O (1)	**2.8**	**1.75**	**166**
C−H···O (2)	**3.7**	**2.55**	**160**
C−H···O (3)	**3.0**	**2.1**	**141**
C−H···O (4)	**2.8**	**1.75**	**153**
C−H···O (1′)	3.4	2.4	180
C−H···O (2′)	4.3	3.4	138
C−H···O (3′)	4.4	3.3	180
C−H···O (4′)	4.1	3.0	170

[a] The favorable lateral carboxylate−CH coupling in the parquet pattern is printed in bold.

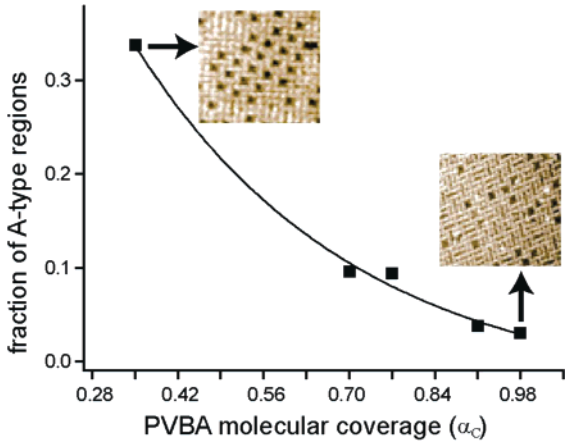

Figure 5. Fraction of the type A regions as a function of the global PVBA coverage. The line is drawn as a guide for the eye. The two insets show typical STM topographs at coverages well below (0.36 α_C) and close to the critical value (0.98 α_C).

to the type A regions. In contrast, the type B regions necessarily comprise both lateral bonding schemes.

Figure 4b shows a tentative model for a hypothetical heterochiral dimer, revealing that the potential binding between the two pyridyl moieties would be even weaker than that of the observed homochiral dimers because of the increased N···H distance if the molecules preserve the energetically favorable adsorption sites. Moreover, Figure 4c depicts a hypothetical model showing the binding between a δ-dimer and a λ-dimer. This configuration is unfavorable compared to the binding in strictly homochiral arrangements modeled in Figure 4a. Thus, the chiral recognition can be readily understood on the basis of the formation of the energetically favored intermolecular hydrogen bonds.

The lateral carboxylate coupling thus naturally explains the existence of voids in the low-density parquet patterns. Chiral resolution occurs up to the critical coverage where the domains consisting of A-type and the B-type regions cover the entire surface. The proportion of type B regions augments with increasing coverage at the expense of type A regions. In Figure 5, the fraction of the type A regions is plotted as a function of the global molecular coverage and the insets show typical topologies for coverages well below and close to the critical value. From the experimental data, the PVBA molecules in the type B regions are more closely packed, ∼0.05 PVBA per Cu atom, compared with the estimated packing density of ∼0.04 PVBA per Cu atom in the type A regions. Hence, the observed trend is attributed to steric constraints at high coverage. The more open type A regions are energetically preferred because of the advantageous lateral coupling.

3.2. Racemic Butterfly Phase above the Critical Coverage α_C. Upon increasing the molecular concentration above the critical value (α_C, 0.05 PVBA per Cu surface atom, corresponding to a surface fully covered with the type B regions described above), we encountered a sharp transition to a new phase. Figure 6a depicts an STM topograph of a sample with a coverage of 1.1 α_C. The parquet pattern has completely vanished, and a regular single phase has developed. This new phase can be similarly obtained by deposition of additional PVBA on top of the homochiral phase and subsequent annealing between 400 and 450 K. The formation of the new "butterfly" phase (named after the underlying motif described below) sets in at the critical coverage α_C, where it intially coexists with the parquet phases until it covers the entire surface for coverages in excess of ∼1.1 α_C.

Despite the frequent domain boundaries encountered, the new phase shows long-range order within the entire domains, in marked contrast to the parquet patterns. As highlighted in Figure 6b, it comprises butterfly-like units made from four PVBA. These features from a regular square lattice where adjacent butterflies are rotated by 90°. The corresponding square unit cell has a size of 3 nm^2 and is oriented along the high-symmetry [001] direction of the Cu(100) substrate, corresponding to a p(12

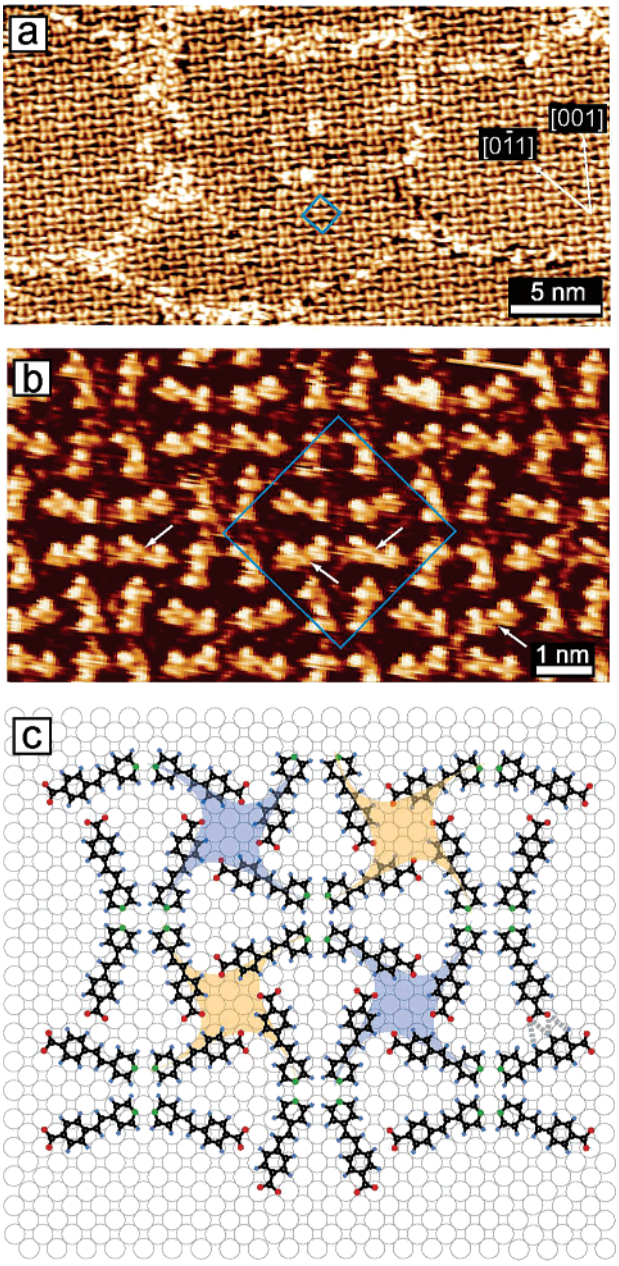

Figure 6. (a,b) STM topography of the butterfly phase obtained for a coverage exceeding the critical value (1.1 α_C, after annealing to 450 K) The squares indicate the superstructure unit cell. In the high-resolution image in (b) orbitals at the ethenylene bridges are signaled by arrows. (c) Tentative model of the racemic layer with propeller features colored according to their turning directions.

$\times$ 12) superstructure. The packing density is 0.055 PVBA per Cu atom (i.e., 10% higher than that of the type B region in the homochiral phase).

The observation of a single phase suggests that mesososcopic chiral resolution and organizational chirality are absent in the new phase. Figure 6b shows high-resolution STM data, where the PVBA species are imaged in the same way as in the homochiral parquet phase. Although the resolution is not as high as in Figure 2b,c, one can distinguish the two protrusions corresponding to the orbital at the ethenylene bridge (cf. white arrows). From a detailed analysis of the data, we concluded that every butterfly unit comprises two λ-PVBA and two δ-PVBA which arrange in a symmetric manner with respect to the [001] and [010] directions. Consequently, the domains are built with a 1:1 mixture of the two PVBA enantiomers (i.e., they represent a racemic phase). This ordering indicates that the higher packing density prevents chiral resolution in the assembly.

A tentative model for the butterfly structure is depicted in Figure 6c, assuming that the PVBA substrate coupling is similar to the one in the parquet patterns. The structure may be viewed as composed of propeller-shaped units. Each unit is made of four PVBA molecules of the same chirality and thus represents a chiral cluster, in which the lateral intermolecular coupling is again due to carboxylate moieties engaged in weak tail-to-side C$-$H$\cdots$O hydrogen bonding (H$\cdots$O distance is 2.4 Å). The overall structure is built by a 1:1 mixture of the propeller units, which are turning in two opposite orientations and form the square pattern highlighted by the colors in the model. Thus, this phase can be considered as racemic mixture. Obviously the propeller units are shaped and squeezed together on the surface as a consequence of the packing requirements at the high molecular density. This is understood as the driving force of the resulting rapprochement between the nitrogen and hydrogen atoms of the pyridyl moiety. Note that a related example of steric repulsive interactions as driving force for self-assembly was recently reported for the case of helicene on Cu(111) at high coverage.[21] With the present system, the steric repulsion is associated with a marked structural transition as the coverage reaches a critical value and the packing requirements shift the subtle balance of the weak forces determining the self-assembly scenario.

4. Conclusion

In conclusion, the study of PVBA molecules on Cu(100) provides new insight into 2D chiral self-assembly phenomena. Upon confinement in 2D PVBA molecules exist in two enantiomeric forms on the surface (δ- and λ-PVBA). From high-resolution STM images the chirality of individual molecules was determined. Up to a critical coverage of 0.05 PVBA per Cu atom, mesoscopic chiral resolution occurs and the subtle balance between lateral intermolecular and molecule$-$substrate interactions leads to the formation of enantiopure δ and λ domains. An abrupt structural transition is observed for coverages exceeding the critical value, where the mesoscopic organizational chirality is suppressed and the molecules assemble in a single homogeneous phase comprising both δ and λ species. The driving force that suppresses the chiral resolution is associated with the packing requirements overriding lateral repulsions at high molecular coverage.

Acknowledgment. We thank Prof. Ch. Cai (University of Houston, Texas) for providing the PVBA molecules. This work was supported by DFG, ESF, and EU.

JA0525049